arXiv:2305.08494v1 [cond-mat.quant-gas] 15 May 2023

Topological two-body bands in a multiband Hubbard model

M. Iskin[1]

[1] *Department of Physics, Koç University, Rumelifeneri Yolu, 34450 Sarıyer, Istanbul, Turkey*

(Dated: September 22, 2024)

In a multiband Hubbard model the self-consistency relations for the two-body bound-state bands are in the form of a nonlinear eigenvalue problem. Assuming that the resultant eigenvectors form an orthonormal set, e.g., in the strong-binding regime, here we reformulate their Berry curvatures and the associated Chern numbers. As an illustration we solve the two-body problem in a Haldane-Hubbard model with attractive onsite interactions, and analyze its topological phase diagrams from weak to strong couplings, i.e., by keeping track of the gap closings in between the low-lying two-body bands. The resultant Chern numbers are consistent with the lobe structure of the phase diagrams in the strong-coupling regime.

I. INTRODUCTION

Topological classification of Bloch bands provides a fresh perspective on modern band theory, with important experimental implications [1]. For instance the Haldane model on a honeycomb lattice stabilizes quantum Hall effect by breaking both time-reversal and inversion symmetries through complex-valued hoppings and sublattice potential, i.e., without the need for the Landau levels that are induced by an external magnetic field [2]. The model features topologically distinct phases of matter with non-zero Chern numbers, making it one of the main workhorses for theoretical research on topological insulators and superconductors. Furthermore its experimental realization using an optical honeycomb lattice is a significant breakthrough in the field of topological matter as the atomic systems offer unprecedented control over the model parameters [3]. Therefore a wide range of topological phases and their associated phenomena are within experimental reach, including the interplay between interactions and topology [4].

Exploring and discovering exotic phases of interacting matter such as fractional Chern and topological Mott insulators remains a primary objective in this field [5, 6]. However, due to the complexity of interacting many-body problems, a bottom-up approach examining the exactly solvable two-body problem in a multiband Hubbard model can sometimes be useful [7]. There are many recent works on various topological aspects of the two-body problem [8–15]. Among them the topological two-boson bound states in the repulsive Haldane-Bose-Hubbard model were analyzed using exact diagonalization in real space [11], and in this paper, we examine the two-body problem for a multiband Fermi-Hubbard model in momentum space. The self-consistency relations for the two-body bound-state bands are in the form of a nonlinear eigenvalue problem [16–18], and we reformulate the Berry curvature and the associated Chern number in the strong-binding regime with the underlying assumption that the resultant eigenvectors form approximately an orthonormal set. As an illustration we construct topological phase diagrams for the attractive Haldane-Hubbard model from weak to strong couplings, and show that the lobe structure of the phase diagram is consistent with the associated Chern numbers in the strong-coupling regime. We would like to emphasize that our formulation is also pertinent to various other physical systems, e.g., in the investigation of flat-band physics in Kagome metals and twisted bilayer graphene, where recent advances in the study of strong-correlation physics have already revealed intriguing connections between topology and electronic properties [19–22].

The rest of the paper is organized as follows. In Sec. II we express the exact solution in the form of a nonlinear eigenvalue problem, and perform its strong-coupling expansion. In Sec. III we derive an effective Hamiltonian for the strongly-bound pairs in a generic two-band model, and benchmark it with the Haldane, Su-Schrieffer-Heeger and Hofstadter models. In Sec. IV we focus on the Haldane-Hubbard model, and analyze its topological phase diagram numerically for the two-body bands. The paper ends with a brief summary of our conclusions in Sec. V, and three Appendices on (A) derivation of the hopping parameters for the effective Hamiltonian, (B) derivation of the Berry curvature for the eigenvectors of the nonlinear eigenvalue problem and (C) application to the isolated flat bands.

II. TWO-BODY BOUND STATES

In this section we consider a generic tight-binding lattice with multiple sublattices, and show that the number of sublattices determines not only the number of Bloch bands but also the number of so-called two-body bound-state bands as follows.

A. One-body problem

The one-body problem in a multiband lattice is described by

$$h_{\sigma\mathbf{k}}\mathbf{f}_{n\sigma\mathbf{k}} = \varepsilon_{n\sigma\mathbf{k}}\mathbf{f}_{n\sigma\mathbf{k}}, \tag{1}$$

where the matrix $h_{\sigma\mathbf{k}}$ represents the Bloch Hamiltonian for the spin-σ particle with momentum $\mathbf{k}$ in the sub-

lattice basis $\alpha = \{A, B, C, \cdots\}$, its eigenvectors $\mathbf{f}_{n\sigma\mathbf{k}} = (n_{A\sigma\mathbf{k}}, n_{B\sigma\mathbf{k}}, n_{C\sigma\mathbf{k}}, \cdots)^{\mathrm{T}}$ with $n_{\alpha\sigma\mathbf{k}} = \langle\alpha|n\sigma\mathbf{k}\rangle$ represent the periodic part of the Bloch states $|n\sigma\mathbf{k}\rangle$ and its eigenvalues $\varepsilon_{n\sigma\mathbf{k}}$ determine the Bloch bands. Here T is the transpose which is in such a way that $\sum_\beta h^{\alpha\beta}_{\sigma\mathbf{k}} n_{\beta\sigma\mathbf{k}} = \varepsilon_{n\sigma\mathbf{k}} n_{\alpha\sigma\mathbf{k}}$. In the presence of two sublattices only, the Bloch Hamiltonian can be written as

$$h_{\sigma\mathbf{k}} = d^0_{\sigma\mathbf{k}}\tau_0 + \mathbf{d}_{\sigma\mathbf{k}} \cdot \boldsymbol{\tau}, \tag{2}$$

where the $\mathbf{k}$ dependences of $d^0_{\sigma\mathbf{k}}$ and $\mathbf{d}_{\sigma\mathbf{k}} = (d^x_{\sigma\mathbf{k}}, d^y_{\sigma\mathbf{k}}, d^z_{\sigma\mathbf{k}})$ are determined by the details of the hopping processes and onsite energies. Here τ_0 is an identity matrix and $\boldsymbol{\tau} = (\tau_x, \tau_y, \tau_z)$ is a vector of Pauli spin matrices for the sublattice sector. The Bloch bands are given by $\varepsilon_{s\sigma\mathbf{k}} = d^0_{\sigma\mathbf{k}} + s d_{\sigma\mathbf{k}}$, where $s = \pm$ denotes the upper and lower bands, and $d_{\sigma\mathbf{k}} = \sqrt{(d^x_{\sigma\mathbf{k}})^2 + (d^y_{\sigma\mathbf{k}})^2 + (d^z_{\sigma\mathbf{k}})^2}$ is the magnitude of $\mathbf{d}_{\sigma\mathbf{k}}$. The sublattice projections of Bloch states $\mathbf{f}_{s\sigma\mathbf{k}} = (s_{A\sigma\mathbf{k}}, s_{B\sigma\mathbf{k}})^{\mathrm{T}}$ can be written as $\mathbf{f}_{+,\sigma\mathbf{k}} = \left(u_{\sigma\mathbf{k}}, v_{\sigma\mathbf{k}} e^{i\varphi_{\sigma\mathbf{k}}}\right)^{\mathrm{T}}$ for the upper band and $\mathbf{f}_{-,\sigma\mathbf{k}} = \left(-v_{\sigma\mathbf{k}} e^{-i\varphi_{\sigma\mathbf{k}}}, u_{\sigma\mathbf{k}}\right)^{\mathrm{T}}$ for the lower band, where $u_{\sigma\mathbf{k}} = \sqrt{(d_{\sigma\mathbf{k}} + d^z_{\sigma\mathbf{k}})/(2d_{\sigma\mathbf{k}})}$ and $v_{\sigma\mathbf{k}} = \sqrt{(d_{\sigma\mathbf{k}} - d^z_{\sigma\mathbf{k}})/(2d_{\sigma\mathbf{k}})}$ are the usual amplitudes and $\varphi_{\sigma\mathbf{k}} = \arg(d^x_{\sigma\mathbf{k}} + i d^y_{\sigma\mathbf{k}})$ is the polar angle on the Bloch sphere. Using the solutions of the one-body problem, next we construct solutions for the low-lying two-body bound states.

B. Nonlinear eigenvalue problem

The two-body problem in a multiband Hubbard model is exactly solvable, and the resultant spectrum can be divided into three distinct set of solutions [16–18]. The first set is the scattering continua, and these states correspond to two unbound (non-interacting) particles. There are $M_b(M_b+1)/2$ possible continua in total where M_b is the number of Bloch bands, i.e., the number of sublattices. The second set is the so-called offsite bound states, and they lie in between the scattering continua. For this reason these states remain weakly bound even in the strongly-interacting regime. The third set is the so-called onsite bound states, and they lie either on top or at the bottom of the two-body spectrum depending on whether the onsite Hubbard interaction is repulsive or attractive, respectively. There are M_b of them for a given center of mass momentum $\mathbf{q}$ of the two particles. These states become strongly bound in the strongly-interacting regime, where they eventually correspond to strongly-localized onsite pairs. In this paper we focus only on this last set of solutions because they give rise to the two-body bands as a function of $\mathbf{q}$.

For the two-body problem between an $\uparrow$ and a $\downarrow$ fermion, the third set can be determined entirely via the self-consistency relation [16, 17]

$$N_{\alpha\mathbf{q}} = \frac{U}{M_c} \sum_{nm\mathbf{k}\beta} \frac{n^*_{\beta\uparrow\mathbf{k}+\mathbf{q}} m^*_{\beta\downarrow-\mathbf{k}} m_{\alpha\downarrow-\mathbf{k}} n_{\alpha\uparrow\mathbf{k}+\mathbf{q}}}{\varepsilon_{n\uparrow\mathbf{k}+\mathbf{q}} + \varepsilon_{m\downarrow-\mathbf{k}} - E_{N\mathbf{q}}} N_{\beta\mathbf{q}}, \tag{3}$$

where $U \geq 0$ is the strength of the attractive onsite Hubbard interaction, M_c is the number of unit cells in the lattice, and $E_{N\mathbf{q}}$ is the energy of the bound state. This expression is also valid for $U < 0$, in which case $-U$ corresponds to the strength of the repulsive onsite Hubbard interaction. One can rewrite it as $\mathbf{G}_{N\mathbf{q}}\mathbf{F}_{N\mathbf{q}} = 0$, and determine $E_{N\mathbf{q}}$ self-consistently through an iterative approach, where $\mathbf{F}_{N\mathbf{q}} = \left(N_{A\mathbf{q}}, N_{B\mathbf{q}}, N_{C\mathbf{q}}, \cdots\right)^{\mathrm{T}}$ represents the bound state $|N\mathbf{q}\rangle$ in the sublattice basis. For a given $\mathbf{q}$, different N corresponds to a self-consistent solution that is determined by setting the first, or second, or third, etc., eigenvalue of the Hermitian matrix $\mathbf{G}_{N\mathbf{q}}$ to be 0. Note that each $E_{N\mathbf{q}}$ solution gives in return a different $\mathbf{G}_{N\mathbf{q}}$ matrix once the self-consistency is achieved.

Equation (3) can also be interpreted as a nonlinear eigenvalue problem

$$H_{N\mathbf{q}}\mathbf{F}_{N\mathbf{q}} = E_{N\mathbf{q}}\mathbf{F}_{N\mathbf{q}}, \tag{4}$$

in such a way that $\sum_\beta H^{\alpha\beta}_{N\mathbf{q}} N_{\beta\mathbf{q}} = E_{N\mathbf{q}} N_{\alpha\mathbf{q}}$. This eigenvalue problem is not in the usual form because the matrix elements

$$H^{\alpha\beta}_{N\mathbf{q}} = \frac{E_{N\mathbf{q}}U}{M_c} \sum_{nm\mathbf{k}} \frac{n^*_{\beta\uparrow\mathbf{k}+\mathbf{q}} m^*_{\beta\downarrow-\mathbf{k}} m_{\alpha\downarrow-\mathbf{k}} n_{\alpha\uparrow\mathbf{k}+\mathbf{q}}}{\varepsilon_{n\uparrow\mathbf{k}+\mathbf{q}} + \varepsilon_{m\downarrow-\mathbf{k}} - E_{N\mathbf{q}}} \tag{5}$$

depend explicitly on the eigenvalue $E_{N\mathbf{q}}$, and hence, it corresponds to a self-consistency relation for each $E_{N\mathbf{q}}$. For instance, in the presence of two sublattices only, the relevant matrix for a given bound-state solution $E_{S\mathbf{q}}$ can be written as

$$H_{S\mathbf{q}} = D^0_{S\mathbf{q}}\tau_0 + \mathbf{D}_{S\mathbf{q}} \cdot \boldsymbol{\tau}, \tag{6}$$

where $D^0_{S\mathbf{q}} = (H^{AA}_{S\mathbf{q}} + H^{BB}_{S\mathbf{q}})/2$, $D^x_{S\mathbf{q}} = \mathrm{Re}H^{BA}_{S\mathbf{q}}$, $D^y_{S\mathbf{q}} = \mathrm{Im}H^{BA}_{S\mathbf{q}}$, and $D^z_{S\mathbf{q}} = (H^{AA}_{S\mathbf{q}} - H^{BB}_{S\mathbf{q}})/2$. Here Re and Im denotes, respectively, the real and imaginary parts. The corresponding eigenvector of $H_{S\mathbf{q}}$ that satisfies the self-consistency relation can be denoted as $\mathbf{F}_{S\mathbf{q}} = \left(S_{A\mathbf{q}}, S_{B\mathbf{q}}\right)^{\mathrm{T}}$. Note that, for a given self-consistent solution $E_{S\mathbf{q}}$, the matrix $H_{S\mathbf{q}}$ has two eigenvalues, but only one of those satisfies the self-consistency relation. The other solution and its eigenvector are irrelevant. Alternatively the self-consistency relations can be written as $E_{S\mathbf{q}} = D^0_{S\mathbf{q}} + S' D_{S\mathbf{q}}$, where $S' = \pm$ and $D_{S\mathbf{q}} = \sqrt{(D^x_{S\mathbf{q}})^2 + (D^y_{S\mathbf{q}})^2 + (D^z_{S\mathbf{q}})^2}$.

For a given $\mathbf{q}$, since each $E_{N\mathbf{q}}$ solution is associated with a different Hermitian matrix $H_{N\mathbf{q}}$, the corresponding eigenvectors $\mathbf{F}_{N\mathbf{q}}$ do not necessarily form an orthonormal set in general. The only exception for this seems to be the strong-binding regime, where the onsite bound states become strongly localized on a single lattice site, i.e., on one of the sublattices, and become approximately orthogonal to each other at finite $|U|$. Note that there are as many two-body bands as the number of sublattices or equivalently as the number of Bloch bands. Thus it may be possible to interpret $H_{N\mathbf{q}}$ as an effective Hamiltonian for the onsite bound states as discussed next.

C. Strong-binding regime

As an illustration here we focus on lattices with a two-point basis for the simplicity of their presentation. A similar analysis can be performed for multiband lattices. It turns out the binding energy is of order $|U|$ in the strong-binding regime when $|U|$ is much larger than the bandwidth of the lowest Bloch band. In general strong binding requires strong interactions in the case of dispersive Bloch bands. However, in the particular case when the lowest (highest) Bloch band is flat and it is separated from the other bands by an energy gap, even an arbitrarily small $U > 0$ ($U < 0$) can be treated as strong-binding regime. In such a case the binding energy of the lowest bound state is known to be of order $|U|/M_b$. Thus isolated flat bands are also amenable to a similar strong-binding expansion when the interactions are weak.

In the strong-coupling regime, the matrix elements of Eq. (6) can be expanded as

$$D^0_{S\mathbf{q}} = -U\left(1 + \frac{\lambda_{1\mathbf{q}}}{E_{S\mathbf{q}}} + \frac{\lambda_{2\mathbf{q}}}{E^2_{S\mathbf{q}}} + \frac{\lambda_{3\mathbf{q}}}{E^3_{S\mathbf{q}}} + \cdots\right), \quad (7)$$

$$D^x_{S\mathbf{q}} + iD^y_{S\mathbf{q}} = -U\left(\frac{\kappa_{2\mathbf{q}}}{E^2_{S\mathbf{q}}} + \frac{\kappa_{3\mathbf{q}}}{E^3_{S\mathbf{q}}} + \cdots\right), \quad (8)$$

$$D^z_{S\mathbf{q}} = -U\left(\frac{\gamma_{1\mathbf{q}}}{E_{S\mathbf{q}}} + \frac{\gamma_{2\mathbf{q}}}{E^2_{S\mathbf{q}}} + \frac{\gamma_{3\mathbf{q}}}{E^3_{S\mathbf{q}}} + \cdots\right), \quad (9)$$

where $\lambda_{i\mathbf{q}}$ and $\gamma_{i\mathbf{q}}$ are real numbers but $\kappa_{i\mathbf{q}}$ is a complex number. After some algebra discussed in Appendix A, these expansion coefficients can be written as

$$\lambda_{1\mathbf{q}} = \frac{1}{M_c}\sum_{\mathbf{k}}\left(d^0_{\uparrow\mathbf{k}+\mathbf{q}} + d^0_{\downarrow-\mathbf{k}}\right), \quad (10)$$

$$\lambda_{2\mathbf{q}} = \frac{1}{M_c}\sum_{\mathbf{k}}\left[\left(d^0_{\uparrow\mathbf{k}+\mathbf{q}} + d^0_{\downarrow-\mathbf{k}}\right)^2 + \left(d^z_{\uparrow\mathbf{k}+\mathbf{q}} + d^z_{\downarrow-\mathbf{k}}\right)^2 + |g_{\uparrow\mathbf{k}+\mathbf{q}}|^2 + |g_{\downarrow-\mathbf{k}}|^2\right], \quad (11)$$

$$\kappa_{2\mathbf{q}} = \frac{2}{M_c}\sum_{\mathbf{k}} g_{\uparrow\mathbf{k}+\mathbf{q}} g_{\downarrow-\mathbf{k}}, \quad (12)$$

$$\gamma_{1\mathbf{q}} = \frac{1}{M_c}\sum_{\mathbf{k}}\left(d^z_{\uparrow\mathbf{k}+\mathbf{q}} + d^z_{\downarrow-\mathbf{k}}\right), \quad (13)$$

$$\gamma_{2\mathbf{q}} = \frac{2}{M_c}\sum_{\mathbf{k}}\left(d^0_{\uparrow\mathbf{k}+\mathbf{q}} + d^0_{\downarrow-\mathbf{k}}\right)\left(d^z_{\uparrow\mathbf{k}+\mathbf{q}} + d^z_{\downarrow-\mathbf{k}}\right), \quad (14)$$

where $g_{\sigma\mathbf{k}} = d^x_{\sigma\mathbf{k}} + id^y_{\sigma\mathbf{k}} = |g_{\sigma\mathbf{k}}|e^{i\varphi_{\sigma\mathbf{k}}}$ is defined for convenience. Typically $\lambda_{1\mathbf{q}} = 0$ when the sublattice potentials are symmetric around 0, and $\gamma_{1\mathbf{q}} = 0 = \gamma_{2\mathbf{q}}$ when the Bloch Hamiltonian exhibits time-reversal symmetry. See Sec. III for example models.

When $\gamma_{1\mathbf{q}} \geq 0$, the bound-state energies are determined by the self-consistency relation $E_{S\mathbf{q}} = D^0_{S\mathbf{q}} + SD_{S\mathbf{q}}$, where $S = \pm$ corresponds to upper and lower two-body bands, respectively. On the other hand $S = \pm$ corresponds to lower and upper two-body bands when $\gamma_{1\mathbf{q}} < 0$. Up to first order in $1/U$, the self-consistency relations lead to $E_{S\mathbf{q}} = -U + \epsilon_{S\mathbf{q}} + \eta_{S\mathbf{q}}/U + \mathcal{O}(1/U^2)$, where $\epsilon_{S\mathbf{q}} = \lambda_{1\mathbf{q}} + S|\gamma_{1\mathbf{q}}|$, and $\eta_{S\mathbf{q}} = (\lambda^2_{1\mathbf{q}} - \lambda_{2\mathbf{q}} + S\sqrt{\gamma^2_{2\mathbf{q}} + |\kappa_{2\mathbf{q}}|^2})/U$ when $\gamma_{1\mathbf{q}} = 0$ but $\eta_{S\mathbf{q}} = \epsilon^2_{S\mathbf{q}} - \lambda_{2\mathbf{q}} - S\gamma_{2\mathbf{q}}|\gamma_{1\mathbf{q}}|/\gamma_{1\mathbf{q}}$ when $\gamma_{1\mathbf{q}} \neq 0$. Up to second order in $1/U$, thus we obtain

$$D^0_{S\mathbf{q}} = -U + \lambda_{1\mathbf{q}} + \frac{\lambda_{1\mathbf{q}}\epsilon_{S\mathbf{q}} - \lambda_{2\mathbf{q}}}{U} + \frac{\lambda_{1\mathbf{q}}(\eta_{S\mathbf{q}} + \epsilon^2_{S\mathbf{q}}) - 2\lambda_{2\mathbf{q}}\epsilon_{S\mathbf{q}} + \lambda_{3\mathbf{q}}}{U^2} + \cdots, \quad (15)$$

$$D^x_{S\mathbf{q}} + iD^y_{S\mathbf{q}} = -\frac{\kappa_{2\mathbf{q}}}{U} - \frac{2\kappa_{2\mathbf{q}}\epsilon_{S\mathbf{q}} - \kappa_{3\mathbf{q}}}{U^2} + \cdots, \quad (16)$$

$$D^z_{S\mathbf{q}} = \gamma_{1\mathbf{q}} + \frac{\gamma_{1\mathbf{q}}\epsilon_{S\mathbf{q}} - \gamma_{2\mathbf{q}}}{U} + \frac{\gamma_{1\mathbf{q}}(\eta_{S\mathbf{q}} + \epsilon^2_{S\mathbf{q}}) - 2\gamma_{2\mathbf{q}}\epsilon_{S\mathbf{q}} + \gamma_{3\mathbf{q}}}{U^2} + \cdots. \quad (17)$$

These expressions can be used to construct an effective Hamiltonian $H_{\mathbf{q}}$ for the onsite bound states in the strong-coupling regime. For instance, when Eqs. (15), (16) and (17) do not depend on S (e.g. when $\lambda_{1\mathbf{q}} = 0 = \gamma_{1\mathbf{q}}$), $H_{\mathbf{q}}$ coincides trivially with $H_{+,\mathbf{q}} = H_{-,\mathbf{q}}$ up to second order in $1/U$. As a non-trivial illustration, next we derive $H_{\mathbf{q}}$ up to first order in $1/U$ for a generic lattice using perturbation theory.

III. EXAMPLE MODELS

Suppose $\gamma_{1\mathbf{q}} \geq 0$ without losing generality so that $S = \pm$ corresponds to upper and lower two-body bands, respectively, and the associated onsite bound states are strongly localized on sublattice A and B, respectively. This is clearly seen in the unperturbed (i.e., $|U| \to \infty$) problem, where sublattices A and B are decoupled from each other [i.e., Eq. (16) $\to 0$)], and the unperturbed two-body band $E^{(0)}_{S\mathbf{q}} = -U + \lambda_{1\mathbf{q}} + S\gamma_{1\mathbf{q}}$ corresponds to a completely localized state on the relevant sublattice. Then the finite-U effects can be taken into account through perturbation theory. For instance, at first order in $1/U$, the matrix elements $H^{\alpha\beta}_{\mathbf{q}}$ of the effective Hamiltonian $H_{\mathbf{q}}$ are such that $H^{AA}_{\mathbf{q}} \equiv H^{AA}_{+,\mathbf{q}} = D^0_{+,\mathbf{q}} + D^z_{+,\mathbf{q}}$, $H^{BB}_{\mathbf{q}} \equiv H^{BB}_{-,\mathbf{q}} = D^0_{-,\mathbf{q}} - D^z_{-,\mathbf{q}}$, and $H^{BA}_{\mathbf{q}} \equiv H^{BA}_{\pm,\mathbf{q}} = D^x_{\pm,\mathbf{q}} + iD^y_{\pm,\mathbf{q}}$. This effective Hamiltonian can be written as $H_{\mathbf{q}} = D^0_{\mathbf{q}}\tau_0 + \mathbf{D}_{\mathbf{q}} \cdot \boldsymbol{\tau}$, where

$$D^0_{\mathbf{q}} = -U + \lambda_{1\mathbf{q}} + \frac{\lambda^2_{1\mathbf{q}} + \gamma^2_{1\mathbf{q}} - \lambda_{2\mathbf{q}}}{U}, \quad (18)$$

$$D^x_{\mathbf{q}} + iD^y_{\mathbf{q}} = -\frac{\kappa_{2\mathbf{q}}}{U}, \quad (19)$$

$$D^z_{\mathbf{q}} = \gamma_{1\mathbf{q}} + \frac{2\lambda_{1\mathbf{q}}\gamma_{1\mathbf{q}} - \gamma_{2\mathbf{q}}}{U} \quad (20)$$

determine its matrix elements. These expressions are readily applicable to any Bloch Hamiltonian with a two-point basis. Some important models are discussed next.

A. Haldane model

In the original Haldane model on a honeycomb lattice with a two-point basis, while the nearest-neighbor (i.e., inter-sublattice) hopping $t_{nn} = t$ is a real parameter, the next-nearest-neighbor (i.e., intra-sublattice) hopping $t_{nnn} = t'e^{i\phi}$ is a complex parameter [2]. Its Bloch Hamiltonian $h_{\sigma\mathbf{k}} \equiv h_{\mathbf{k}}$ is such that $d^0_{\mathbf{k}} = -2t'\cos\phi\sum_{j=1}^3\cos(\mathbf{k}\cdot\boldsymbol{\nu_j})$, $d^x_{\mathbf{k}} + id^y_{\mathbf{k}} = -t\sum_{j=1}^3 e^{i\mathbf{k}\cdot\boldsymbol{e_j}}$ and $d^z_{\mathbf{k}} = \delta - 2t'\sin\phi\sum_{j=1}^3\sin(\mathbf{k}\cdot\boldsymbol{\nu_j})$, where δ is the onsite energy difference between sublattices. Here we define $\boldsymbol{e_1} = (0,a)$, $\boldsymbol{e_2} = (-\sqrt{3}a/2, -a/2)$ and $\boldsymbol{e_3} = -(\boldsymbol{e_1} + \boldsymbol{e_2}) = (\sqrt{3}a/2, -a/2)$ for the nearest-neighbor hoppings, and similarly $\boldsymbol{\nu_1} = (\sqrt{3}a, 0)$, $\boldsymbol{\nu_2} = (-\sqrt{3}a/2, 3a/2)$ and $\boldsymbol{\nu_3} = -(\boldsymbol{\nu_1} + \boldsymbol{\nu_2}) = (-\sqrt{3}a/2, -3a/2)$ for the next-nearest-neighbor hoppings, where a is the lattice spacing. Its Brillouin zone has the shape of a hexagon, and it is such that the K and K′ valleys are at $\mathbf{K} = [4\pi/(3\sqrt{3}a), 0]$ and $\mathbf{K}' = [2\pi/(3\sqrt{3}a), 2\pi/(3a)]$ points, respectively.

After some tedious bookkeeping, one can show that the expansion coefficients for the two-body problem are $\lambda_{1\mathbf{q}} = 0$, $\lambda_{2\mathbf{q}} = 6t^2 + 12t'^2 + 4\delta^2 + 4t'^2\cos(2\phi)\sum_{j=1}^3\cos(\mathbf{q}\cdot\boldsymbol{\nu_j})$, $\kappa_{2\mathbf{q}} = 2t^2\sum_{j=1}^3 e^{i\mathbf{q}\cdot\boldsymbol{e_j}}$, $\gamma_{1\mathbf{q}} = 2\delta$ and $\gamma_{2\mathbf{q}} = 4t'^2\sin(2\phi)\sum_{j=1}^3\sin(\mathbf{q}\cdot\boldsymbol{\nu_j})$. Thus the effective Hamiltonian for the onsite bound states is described by $D^0_{\mathbf{q}} = -U - \Lambda - 2T'\cos\Phi\sum_{j=1}^3\cos(\mathbf{q}\cdot\boldsymbol{\nu_j})$, $D^x_{\mathbf{q}} + iD^y_{\mathbf{q}} = -T\sum_{j=1}^3 e^{i\mathbf{q}\cdot\boldsymbol{e_j}}$ and $D^z_{\mathbf{q}} = \Delta - 2T'\sin\Phi\sum_{j=1}^3\sin(\mathbf{q}\cdot\boldsymbol{\nu_j})$, where $\Lambda = (6t^2 + 12t'^2)/U$ is an onsite energy offset, $T = 2t^2/U$ is the effective nearest-neighbor hopping parameter, $T' = 2t'^2/U$ is the amplitude and $\Phi = 2\phi$ is the phase of the effective next-nearest-neighbor hopping parameter, and $\Delta = 2\delta$ is the effective onsite energy difference between sublattices. These effective parameters are consistent with the recent literature [11] [23].

Note that $\Lambda = 2(z_{nn}t^2 + z_{nnn}t'^2)/U$, where $z_{nn} = 3$ is the nearest-neighbor coordination number and $z_{nnn} = 4$ is the next-nearest-neighbor coordination number. The origin of such a $\mathbf{q}$-independent onsite energy offset is as follows. When a bound state breaks up at a cost of binding energy U in the denominator, one of its constituents can hop to a neighboring site and then come back to the original site to recombine, leading to $t_\sigma^2 = t^2$ in the numerator. Thus the center of mass of the pair does not play a role in this process. The coordination numbers appear because such a process can happen with all neighboring sites. The factor of 2 accounts for the spin. On the other hand the effective hopping parameters are $\mathbf{q}$ dependent because when a bound state breaks up and one of its constituents hops to a neighboring site, the other particle follows it and hops to the same site, leading to $t_\uparrow t_\downarrow = t^2$ in the numerator. This is the only physical mechanism for a strongly-bound pair of particles to move in the Hubbard model.

B. Su-Schrieffer-Heeger-Hubbard model

In the Su–Schrieffer–Heeger model on a linear chain with a two-point basis, while the onsite energy difference between sublattices and the intra-sublattice hopping parameters are set to 0, the inter-sublattice hopping parameters alternate between t_L and t_R in the lattice [24]. Its Bloch Hamiltonian $h_{\sigma\mathbf{k}} \equiv h_{\mathbf{k}}$ is such that $d^0_k = 0 = d^z_k$, $d^x_k = -t_L - t_R\cos(ka)$ and $d^y_k = -t_R\sin(ka)$, where a is the lattice spacing, $-\pi/a \le k < \pi/a$ defines the Brillouin zone, and t_L and t_R are real hopping parameters to the left and right of sublattice A, respectively. The Bloch bands can be written as $\varepsilon_{sk} = s\sqrt{t_L^2 + t_R^2 + 2t_Lt_R\cos(ka)}$.

After some simple algebra, one can show that the expansion coefficients for the two-body problem are $\lambda_{1q} = 0 = \gamma_{1q} = \gamma_{2q}$ due to particle-hole and time-reversal symmetries, $\lambda_{2q} = 2t_L^2 + 2t_R^2$ and $\kappa_{2q} = 2t_L^2 + 2t_R^2e^{iqa}$. Thus the effective Hamiltonian for the onsite bound states is described by $D^0_q = -U - \Lambda$, $D^x_q + iD^y_q = -T_L - T_Re^{iqa}$ and $D^z_q = 0$, where $\Lambda = (2t_L^2 + 2t_R^2)/U$ is an onsite energy offset, and $T_L = 2t_L^2/U$ and $T_R = 2t_R^2/U$ are the effective nearest-neighbor hopping parameters. These effective parameters are consistent with the recent literature [25, 26]. Note that $\Lambda = 2(z_Lt_L^2 + z_Rt_R^2)/U$, where $z_L = 1$ and $z_R = 1$ are the corresponding coordination numbers to the left and to the right, respectively. Thus, similar to the Bloch bands, the two-body bands can be written as $E_{Sq} = -U - \Lambda + S\sqrt{T_L^2 + T_R^2 + 2T_LT_R\cos(qa)}$.

C. Hofstadter-Hubbard model at $\alpha_{\sigma B} = 1/2$

The Hofstadter model on a square lattice with nearest-neighbor hoppings t is described by a two-point basis when the magnetic flux quanta per unit cell is $\alpha_{\sigma B} = B_0a^2/\phi_0 = 1/2$ [27–29]. Here B_0 is the strength of the perpendicular magnetic field, a is the lattice spacing, and ϕ_0 is the magnetix-flux quantum. Its Bloch Hamiltonian $h_{\sigma\mathbf{k}} \equiv h_{\mathbf{k}}$ is such that $d^0_{\mathbf{k}} = 0$, $d^x_{\mathbf{k}} = -t - t\cos(2k_xa)$, $d^y_{\mathbf{k}} = -t\sin(2k_xa)$, and $d^z_{\mathbf{k}} = 2t\cos(k_ya)$, where $-\pi/(2a) \le k_x < \pi/(2a)$ and $-\pi/a \le k_y < \pi/a$ defines the magnetic Brillouin zone.

After some simple algebra, one can show that the expansion coefficients for the two-body problem are $\lambda_{1\mathbf{q}} = 0 = \gamma_{1\mathbf{q}} = \gamma_{2\mathbf{q}}$ due to particle-hole and time-reversal symmetries, $\lambda_{2\mathbf{q}} = 8t^2 + 4t^2\cos(q_ya)$ and $\kappa_{2\mathbf{q}} = 2t^2 + 2t^2e^{i2q_xa}$. Thus the effective Hamiltonian for the onsite bound states is described by $D^0_{\mathbf{q}} = -U - \Lambda - 2T\cos(q_ya)$, $D^x_{\mathbf{q}} + iD^y_{\mathbf{q}} = -2T\cos(q_xa)e^{iq_xa}$ and $D^z_{\mathbf{q}} = 0$, where $\Lambda = 8t^2/U$ is an onsite energy offset and $T = 2t^2/U$ is the effective nearest-neighbor hopping parameter. Note that $\Lambda = 2z_{nn}t^2/U$ where $z_{nn} = 4$ is the nearest-neighbor coordination number. Thus the two-body bands can be written as $E_{S\mathbf{q}} = -U - \Lambda - 2T[-S\cos(q_xa) + \cos(q_ya)]$. Apart from a constant shift, it is pleasing to see that they together correspond to a single cosine band

$-2T[\cos(q_x a) + \cos(q_y a)]$ in the usual (non-magnetic) Brillouin zone of a square lattice. This is physically expected because the effective magnetic flux seen by the strongly-bound pair of particles is $\alpha_B = \alpha_{\uparrow B} + \alpha_{\downarrow B} = 1$, and the usual Hofstadter butterfly is known to be symmetric around $\alpha_{\sigma B} = 1/2$, i.e., the spectrum for $\alpha_B = 1$ is equivalent to the non-magnetic spectrum at $\alpha_B = 0$. In fact, starting with $\alpha_{\uparrow B} = 1/2 = -\alpha_{\downarrow B}$, one can easily verify that the resultant effective Hamiltonian is identical to the one given above. This is simply because $h_{\sigma \mathbf{k}}$ does not depend on the sign of $\alpha_{\sigma B} = \pm 1/2$, and always exhibits time-reversal symmetry [30].

IV. TOPOLOGICAL PHASE DIAGRAM

As discussed in the introduction, topological characterization of Bloch bands offers a new perspective on modern band theory. Similarly it may prove useful to construct and characterize the topological phase diagram of the two-body bands. As an illustration next we apply Eq. (3), or equivalently Eq. (4), to the Haldane-Hubbard model from weak to strong couplings.

A. Haldane-Hubbard model

In the original Haldane model that is introduced in Sec. III A, the energy gap between the upper and lower Bloch bands closes at either K or K′ valley, where $d^0_{\mathbf{k}} = 0 = d^x_{\mathbf{k}} = d^y_{\mathbf{k}}$ and $d^z_{\mathbf{k}} = \delta \pm 3\sqrt{3}t' \sin\phi$. Here $\pm$ refers to $\mathbf{K}$ and $\mathbf{K}'$ points, respectively. It turns out while the system is a topological Chern insulator with Chern number $|C_s| = 1$ when $|\delta| < 3\sqrt{3}|t' \sin\phi|$, it is a trivial insulator with $|C_s| = 0$ when $|\delta| > 3\sqrt{3}|t' \sin\phi|$. Thus a topological transition occurs at $|\delta| = 3\sqrt{3}|t' \sin\phi|$, i.e., when there is a band crossing in the system [2].

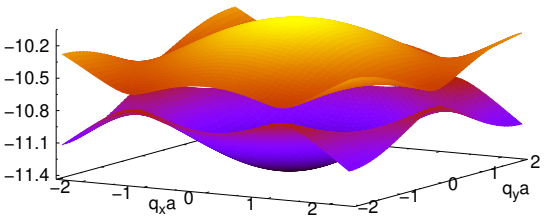


FIG. 1. Upper and lower two-body bands correspond to $E_{+,\mathbf{q}}$ and $E_{-,\mathbf{q}}$, respectively, for the Haldane-Hubbard model in units of t. The band gap occurs either at point $\mathbf{K}$ or $\mathbf{K}'$. Here $t'/t = 0.2$, $\phi = \pi/4$ and $U = 10t$.

As illustrated in Fig. 1, the two-body bands look very similar to the underlying Bloch bands. Accordingly the topological phase diagram of the two-body bands can also be traced by keeping track of their gap closings at the K and K′ valleys. For instance, in the strong-coupling regime when $U/t \gg 1$, one finds $D^0_{\mathbf{q}} = 0 = D^x_{\mathbf{q}} = D^y_{\mathbf{q}}$ but $D^z_{\mathbf{q}} = \Delta \pm 3\sqrt{3}T' \sin\Phi$ at the $\mathbf{K}$ and $\mathbf{K}'$ points, respectively. Thus, analogous to the underlying Bloch bands, while the paired system is expected to be a topological Chern insulator with $|C_S| = 1$ when $|\Delta| < 3\sqrt{3}|T' \sin\Phi|$, it is expected to be a trivial insulator with $|C_S| = 0$ when $|\Delta| > 3\sqrt{3}|T' \sin\Phi|$. The topological transition is expected to occur at $|\Delta| = 3\sqrt{3}|T' \sin\Phi|$.

In Fig. 2 we present the local band gap $E_{+,\mathbf{q}} - E_{-,\mathbf{q}}$ between the two-body bands as a function of phase ϕ of the next-nearest-neighbor hopping t' and the onsite energy difference δ between sublattices. Here we set $t'/t = 0.2$ in all figures, where the upper and lower rows correspond to the local band gaps at points $\mathbf{q} = \mathbf{K}$ and $\mathbf{q} = \mathbf{K}'$, respectively, and different columns correspond to $U/t = \{10, 30, 500\}$. The local band gaps vanish along the white-dotted contours within the narrow black strips. Since the global band gap is minimum of the local band gaps, superposition of white contours determines the location of the vanishing global band gap. For a given $\mathbf{K}$ or $\mathbf{K}'$, each strip has one primary (i.e., larger) and one secondary (i.e., smaller) lobe as a function of $0 \leq \phi < 2\pi$. The secondary lobes are as large as the primary ones only in the strong-coupling regime, and this is in perfect agreement with our strong-coupling analysis.

In the case of $U = 500t$, the period $\pi/2$ and the amplitude $3\sqrt{3}(0.2)^2 t/500 \approx 0.00042t$ of the oscillation that is produced by the combined strips (i.e., superposition of the white-dotted contours that are shown in $\mathbf{K}$ and $\mathbf{K}'$) match very well with our gap closing condition $\delta = 3\sqrt{3}|\sin(2\phi)|t'^2/U$ derived above. However, in the case of $U = 30t$, the oscillation of the combined strips has a period of 2π, and the amplitudes of the primary and secondary lobes deviate substantially from our strong-coupling prediction $0.0069t$. This deviation shows that the higher-order corrections to the effective Hamiltonian play a crucial role in determining the phase boundary. It is pleasing to see that our exact results coming out of Eq. (3) are in full agreement with the recent results that are based on exact diagonalization in real space [11]. There the effective Hamiltonian is derived up to third order in $1/U$, showing that the two-body bound states are described by a generalized Haldane model in general [31]. When U is finite, the amplitudes and phases of the effective next-nearest-neighbor hopping parameter turn out to be different for different sublattices, i.e., one has to consider $T_{nnn} = T'_{AA} e^{i\Phi_A}$ and $T_{nnn} = T'_{BB} e^{i\Phi_B}$ for intra-sublattice hoppings where $T'_{AA} \neq T'_{BB}$ and $\Phi_A \neq \Phi_B$ have much more complicated dependences on t, t', ϕ, δ and U [11].

Furthermore Fig. 2 shows that the secondary lobes already become small when the interaction is lowered down to $U = 10t$. As they start disappearing towards the weakly-interacting regime (e.g., when $U \lesssim 5t$ not shown),

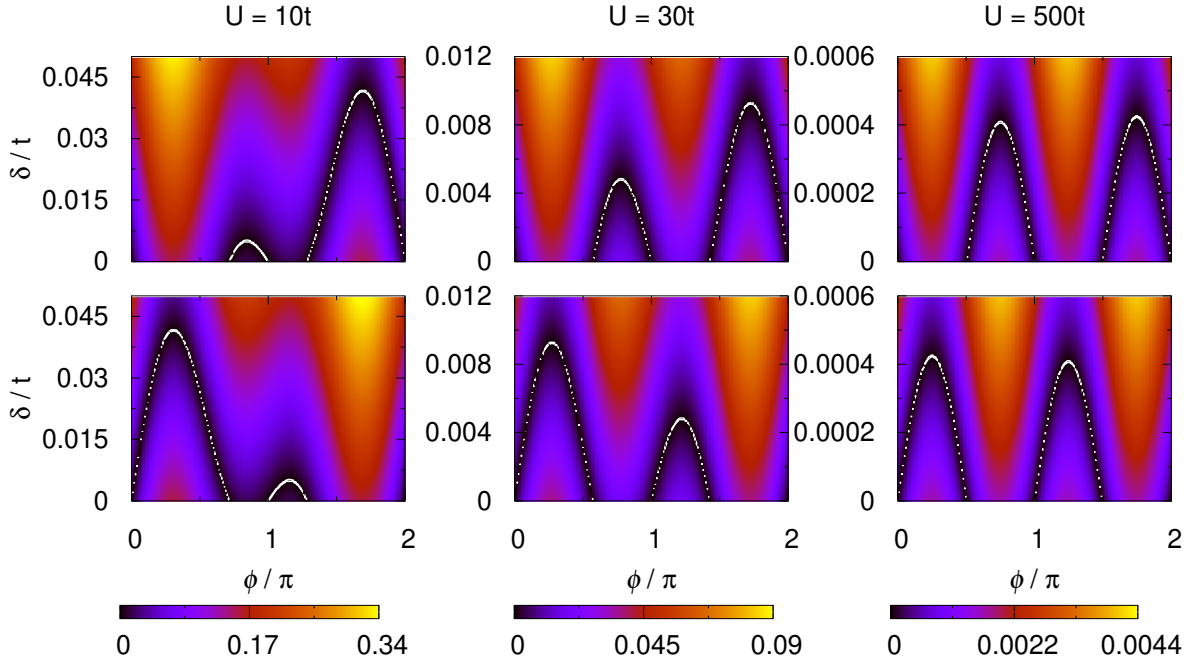


FIG. 2. The local band gap $E_{+,\mathbf{q}} - E_{-,\mathbf{q}}$ (in units of t) between the two-body bands as a function of phase ϕ (in units of π) of the next-nearest-neighbor hopping t' and the onsite energy difference δ (in units of t) between sublattices. Upper and lower rows correspond to the local band gaps at point $\mathbf{K}$ and $\mathbf{K}'$, respectively, when $U/t = \{10, 30, 500\}$. Here $t'/t = 0.2$ is fixed in all figures. The local band gaps vanish along the white-dotted contours within the narrow black strips. For any given U, since the global band gap is minimum of the two, increasing δ closes and reopens the band gap either at point $\mathbf{K}$ or $\mathbf{K}'$ depending on ϕ. Thus superposition of white contours determines the critical boundary for the topological phase transition [11]. When $U = 500t$ and $\delta = 0$, the Chern numbers of the upper and lower two-body bands change from ± 1 in $0 < \phi < \pi/2$, to ∓ 1 in $\pi/2 < \phi < \pi$, to ± 1 in $\pi < \phi < 3\pi/2$, and to ∓ 1 in $3\pi/2 < \phi < 2\pi$.

the lobe structure resembles to that of Bloch bands, i.e., the primary lobe of $\mathbf{K}$ extents from $\phi = 0$ to π and that of $\mathbf{K}'$ extents from π to 2π. This is in such a way that the oscillation of the combined strips has a period of π. Thus both the amplitude and the width of the primary lobes grow in size with decreasing interactions. Next we calculate the Chern number of the two-body bands in the strong-coupling regime and show that it is consistent with the resultant lobe structure.

B. Chern number

The Berry curvature $\Omega_{S\mathbf{q}}$ of the two-body eigenvector $\mathbf{F}_{S\mathbf{q}}$ is derived in the Appendix B. Under the restrictive assumption that the two-body bound states $|S\mathbf{q}\rangle$ are orthonormal to each other, i.e., when the identity operator $\mathcal{I} = |+,\mathbf{q}\rangle\langle+,\mathbf{q}| + |-,\mathbf{q}\rangle\langle-,\mathbf{q}|$ is approximately satisfied, for every $\mathbf{q}$, there we show that

$$\Omega_{S\mathbf{q}} = -2\mathrm{Im}\frac{\langle S\mathbf{q}|\partial_x H_{S\mathbf{q}}|-S,\mathbf{q}\rangle\langle -S,\mathbf{q}|\partial_y H_{S\mathbf{q}}|-S,\mathbf{q}\rangle}{(E_{S\mathbf{q}} - E_{-S,\mathbf{q}})^2}. \tag{21}$$

Here $H_{S\mathbf{q}}$ is defined by Eq. (6) and ∂_j stands for $\partial/\partial q_j$. Then the Chern number of the two-body bands is given by the usual expression $C_S = \frac{2\pi}{L^2}\sum_{\mathbf{q}}\Omega_{S\mathbf{q}}$, where $L_x = L_y = L \gg a$ is the side-length of the square-shaped lattice. In the case of Haldane model, L and M_c are such that $M_c = 2L^2/(3\sqrt{3}a^2)$, i.e., dividing the area $8\pi^2/(3\sqrt{3}a^2)$ of the hexagon-shaped Brillouin zone to the area $4\pi^2/L^2$ per $\mathbf{q}$ state gives the number M_c of $\mathbf{q}$ states (per band) in the Brillouin zone. Unlike that of the Bloch bands, we note that $\Omega_{+,\mathbf{q}}$ and $-\Omega_{-,\mathbf{q}}$ are not necessarily equal to each other by construction because $H_{+,\mathbf{q}}$ and $H_{-,\mathbf{q}}$ are different.

Our numerical calculations show that the orthonormality condition is well-satisfied in the strong-coupling regime. For instance when $\delta = 0$ and $\phi = \pi/4$, we find that the inner product $|\langle+,\mathbf{q}|-,\mathbf{q}\rangle|$ is bounded approximately by $\{3\times10^{-8}, 10^{-4}, 7\times10^{-4}, 2\times10^{-3}\}$ (i.e., for every $\mathbf{q}$ in the Brillouin zone) when $U/t = \{500, 30, 15, 10\}$, respectively. The corresponding Chern numbers for the upper ($S = +$) and lower ($S = -$) two-body bands are $C_+ = 0.994$ and $C_- = -0.994$ for $U = 500t$, $C_+ = 1.03$ and $C_- = -1.02$ for $U = 30t$, $C_+ = 1.15$ and $C_- = -1.09$ for $U = 15t$, and $C_+ = 1.42$ and $C_- = -1.21$ for $U = 10t$. When $\phi = 7\pi/4$, we confirm that all of these Chern numbers simply change signs with exactly the same magnitudes. Similarly when $\delta = 0$ and $\phi = 3\pi/4$, we find that the inner product is bounded approximately by $\{3\times10^{-8}, 10^{-4}, 10^{-3}, 3\times10^{-3}\}$ when $U/t = \{500, 30, 15, 10\}$, respectively. The correspond-

ing Chern numbers are $C_+ = -0.994$ and $C_- = 0.994$ for $U = 500t$, $C_+ = -1.02$ and $C_- = 1.01$ for $U = 30t$, $C_+ = -1.08$ and $C_- = 1.05$ for $U = 15t$, and $C_+ = -0.75$ and $C_- = 0.72$ for $U = 10t$. When $\phi = 5\pi/4$, we again confirm that these Chern numbers also change signs with exactly the same magnitudes.

As long as lowering U/t from 500 to 10 does not open or close any energy gap, e.g., Fig. 2 shows that this is the case when $\delta = 0$ and $\phi = \{\pi/4, 3\pi/4, 5\pi/4, 7\pi/4\}$, the associated Chern number C_S cannot change and must remain invariant for a given lobe. This is not the case in our numerical calculations because the orthonormality condition progressively fails more and more at lower U values. Thus our approach is by construction not expected to reproduce the correct $|C_S| = 1$ in the weak-coupling regime. On the other hand, we use roughly 2000 mesh points and distribute them uniformly in the Brillouin zone in our numerical calculations, and increasing the mesh size may give slightly better results in the strong-coupling regime, e.g., when $U = 500t$ or $U = 30t$. This is because since the Berry curvature $\Omega_{S\mathbf{q}}$ makes a much larger contribution to C_S in the vicinity of $\mathbf{K}$ and $\mathbf{K}'$ points, increasing the mesh size must eventually give $|C_S| = 1$ up to a very high precision once the effective Hamiltonian discussed in Sec. III A becomes applicable.

V. CONCLUSION

In summary here we studied the two-body problem in a Haldane-Hubbard model, and constructed its topological phase diagrams as a function of interaction strength, by keeping track of the gap closings in between the two-body bands. For a given center of mass momentum, the two-body bands are determined by a nonlinear eigenvalue problem, and its self-consistent solutions are obtained numerically through an iterative approach. We found that while the lobe structure of the weakly-interacting phase diagram resembles to that of the Bloch bands, two additional lobes appear and grow gradually with increasing interactions. Our strong-coupling analysis is in perfect agreement with the topological phase diagram, where an effective Hamiltonian is derived for the two-body bands through perturbation theory. In addition, assuming that the eigenvectors of the nonlinear eigenvalue problem form an orthonormal set, we reformulated the Berry cuvature and the associated Chern number. This assumption is typically fulfilled in the strongly-interacting regime, where, e.g., the resultant Chern numbers are again consistent with the lobe structure in the Haldane-Hubbard model. As an outlook, calculation of the correct Chern numbers in the weak-coupling regime is indeed an interesting area of investigation. This may be achieved via an alternative formulation that is based only on one of eigenvectors of the nonlinear eigenvalue problem without an explicit reference to the other eigenvectors or to the orthonormality condition. For instance Ref. [32] offers such a promising approach.

ACKNOWLEDGMENTS

The author acknowledges funding from TÜBİTAK.

Appendix A: Expansion coefficients in Sec. II C

In the strong-coupling regime when the binding energy is much larger than the single-particle energies, i.e., when $|x| \ll 1$ with $x = (\varepsilon_{s\uparrow\mathbf{k}+\mathbf{q}} + \varepsilon_{s'\downarrow-\mathbf{k}})/E_{S\mathbf{q}}$, the matrix elements given in Eq. (5) can be expanded as a geometric series using $1/(1-x) = 1+x+x^2+\cdots$. For instance, in the expansion of the diagonal elements $H^{AA}_{S\mathbf{q}}$ and $H^{BB}_{S\mathbf{q}}$, the zeroth-order terms follow from $\sum_{ss'} |s_{A\uparrow\mathbf{k}+\mathbf{q}}|^2 |s'_{A\downarrow-\mathbf{k}}|^2 = 1 = \sum_{ss'} |s_{B\uparrow\mathbf{k}+\mathbf{q}}|^2 |s'_{B\downarrow-\mathbf{k}}|^2$, the first-order terms follow from $\sum_{ss'} |s_{A\uparrow\mathbf{k}+\mathbf{q}}|^2 |s'_{A\downarrow-\mathbf{k}}|^2 (\varepsilon_{s\uparrow\mathbf{k}+\mathbf{q}} + \varepsilon_{s'\downarrow-\mathbf{k}}) = d^0_{\uparrow\mathbf{k}+\mathbf{q}} + d^z_{\uparrow\mathbf{k}+\mathbf{q}} + d^0_{\downarrow-\mathbf{k}} + d^z_{\downarrow-\mathbf{k}}$ and $\sum_{ss'} |s_{B\uparrow\mathbf{k}+\mathbf{q}}|^2 |s'_{B\downarrow-\mathbf{k}}|^2 (\varepsilon_{s\uparrow\mathbf{k}+\mathbf{q}} + \varepsilon_{s'\downarrow-\mathbf{k}}) = d^0_{\uparrow\mathbf{k}+\mathbf{q}} - d^z_{\uparrow\mathbf{k}+\mathbf{q}} + d^0_{\downarrow-\mathbf{k}} - d^z_{\downarrow-\mathbf{k}}$, and the second-order terms follow from $\sum_{ss'} |s_{A\uparrow\mathbf{k}+\mathbf{q}}|^2 |s'_{A\downarrow-\mathbf{k}}|^2 (\varepsilon_{s\uparrow\mathbf{k}+\mathbf{q}} + \varepsilon_{s'\downarrow-\mathbf{k}})^2 = (d^0_{\uparrow\mathbf{k}+\mathbf{q}} + d^0_{\downarrow-\mathbf{k}}) + d^2_{\uparrow\mathbf{k}+\mathbf{q}} + d^2_{\downarrow-\mathbf{k}} + 2d^0_{\uparrow\mathbf{k}+\mathbf{q}}(d^z_{\uparrow\mathbf{k}+\mathbf{q}} + d^z_{\downarrow-\mathbf{k}}) + 2d^0_{\downarrow-\mathbf{k}}(d^z_{\uparrow\mathbf{k}+\mathbf{q}} + d^z_{\downarrow-\mathbf{k}}) + 2d^z_{\uparrow\mathbf{k}+\mathbf{q}} d^z_{\downarrow-\mathbf{k}}$ and $\sum_{ss'} |s_{B\uparrow\mathbf{k}+\mathbf{q}}|^2 |s'_{B\downarrow-\mathbf{k}}|^2 (\varepsilon_{s\uparrow\mathbf{k}+\mathbf{q}} + \varepsilon_{s'\downarrow-\mathbf{k}})^2 = (d^0_{\uparrow\mathbf{k}+\mathbf{q}} + d^0_{\downarrow-\mathbf{k}}) + d^2_{\uparrow\mathbf{k}+\mathbf{q}} + d^2_{\downarrow-\mathbf{k}} - 2d^0_{\uparrow\mathbf{k}+\mathbf{q}}(d^z_{\uparrow\mathbf{k}+\mathbf{q}} + d^z_{\downarrow-\mathbf{k}}) - 2d^0_{\downarrow-\mathbf{k}}(d^z_{\uparrow\mathbf{k}+\mathbf{q}} + d^z_{\downarrow-\mathbf{k}}) + 2d^z_{\uparrow\mathbf{k}+\mathbf{q}} d^z_{\downarrow-\mathbf{k}}$. Here we made frequent use of the normalization condition $u^2_{\sigma\mathbf{k}} + v^2_{\sigma\mathbf{k}} = 1$ for the Bloch eigenvectors. Similarly, in the expansion of the off-diagonal elements $H^{AB}_{S\mathbf{q}} = (H^{BA}_{S\mathbf{q}})^*$, the trivial zeroth-order terms follow from $\sum_{ss'} s^*_{A\uparrow\mathbf{k}+\mathbf{q}} s'^*_{A\downarrow-\mathbf{k}} s_{B\uparrow\mathbf{k}+\mathbf{q}} s'_{B\downarrow-\mathbf{k}} = 0$, the trivial first-order terms follow from $\sum_{ss'} s^*_{A\uparrow\mathbf{k}+\mathbf{q}} s'^*_{A\downarrow-\mathbf{k}} s_{B\uparrow\mathbf{k}+\mathbf{q}} s'_{B\downarrow-\mathbf{k}} (\varepsilon_{s\uparrow\mathbf{k}+\mathbf{q}} + \varepsilon_{s'\downarrow-\mathbf{k}}) = 0$, and the non-trivial second-order terms follow from $\sum_{ss'} s^*_{A\uparrow\mathbf{k}+\mathbf{q}} s'^*_{A\downarrow-\mathbf{k}} s_{B\uparrow\mathbf{k}+\mathbf{q}} s'_{B\downarrow-\mathbf{k}} (\varepsilon_{s\uparrow\mathbf{k}+\mathbf{q}} + \varepsilon_{s'\downarrow-\mathbf{k}})^2 = 2g_{\uparrow\mathbf{k}+\mathbf{q}} g_{\downarrow-\mathbf{k}}$. Here we note that $s^*_{A\uparrow\mathbf{k}+\mathbf{q}} s'^*_{A\downarrow-\mathbf{k}} s_{B\uparrow\mathbf{k}+\mathbf{q}} s'_{B\downarrow-\mathbf{k}} = -g_{\uparrow\mathbf{k}+\mathbf{q}} g_{\downarrow-\mathbf{k}} (-1)^{\delta_{ss'}} / (4 d_{\uparrow\mathbf{k}+\mathbf{q}} d_{\downarrow-\mathbf{k}})$ in such a way that $\sum_{ss'} (-1)^{\delta_{ss'}} = 0$ leads to the zeroth-order result, $\sum_{ss'} (\varepsilon_{s\uparrow\mathbf{k}+\mathbf{q}} + \varepsilon_{s'\downarrow-\mathbf{k}}) (-1)^{\delta_{ss'}} = 0$ leads to the first-order result, and $\sum_{ss'} (\varepsilon_{s\uparrow\mathbf{k}+\mathbf{q}} + \varepsilon_{s'\downarrow-\mathbf{k}})^2 (-1)^{\delta_{ss'}} = -8 d_{\uparrow\mathbf{k}+\mathbf{q}} d_{\downarrow-\mathbf{k}}$ leads to the second-order result.

Appendix B: Berry curvature in Sec. IV B

Unlike the one-body problem, the two-body bands $E_{N\mathbf{q}}$ and their corresponding eigenstates $|N\mathbf{q}\rangle$ are determined by the nonlinear eigenvalue problem given in Eq. (4). For this reason the standard formulation of the Berry curvature is not applicable here. In this Appendix we formulate the Berry curvature of the two-body bands by following closely the footsteps of Berry in his seminal paper [33]. However, it is important to emphasize that the derivation below is not general, and it only applies when the self-consistent solutions for the eigenvec-

tors $|N\mathbf{q}\rangle$ form an orthonormal set, i.e., when the identity operator $\mathcal{I} = \sum_N |N\mathbf{q}\rangle\langle N\mathbf{q}|$ is satisfied, for every $\mathbf{q}$. Our numerical calculations suggest that this condition can approximately be satisfied in the strong-coupling (i.e., $|U|/t \gg 1$) regime once the bound states localize strongly on one of the sublattices. In addition our numerical calculations show that it is also approximately satisfied in the weak-coupling (i.e., $|U|/t \to 0$) limit when the lowest or highest Bloch band is flat. See also Appendix C below.

The Berry connection of the two-body states is defined as $\mathcal{A}_{N\mathbf{q}} = i\langle N\mathbf{q}|\boldsymbol{\nabla} N\mathbf{q}\rangle = -\mathrm{Im}\langle N\mathbf{q}|\boldsymbol{\nabla} N\mathbf{q}\rangle$, where the second equality follows because the inner product is an imaginary number due to $\boldsymbol{\nabla}\langle N\mathbf{q}|N\mathbf{q}\rangle = 0$ for the normalized states. Then the Berry curvature of the two-body states is $\boldsymbol{\Omega}_{N\mathbf{q}} = \boldsymbol{\nabla}\times\mathcal{A}_{N\mathbf{q}} = -\mathrm{Im}\langle\boldsymbol{\nabla} N\mathbf{q}|\times|\boldsymbol{\nabla} N\mathbf{q}\rangle$, where the cross product is between three components of bra and ket vectors. By acting $\boldsymbol{\nabla}$ on the nonlinear eigenvalue Eq. (4), one obtains $(H_{N\mathbf{q}} - E_{N\mathbf{q}})|\boldsymbol{\nabla} N\mathbf{q}\rangle = (\boldsymbol{\nabla} E_{N\mathbf{q}} - \boldsymbol{\nabla} H_{N\mathbf{q}})|N\mathbf{q}\rangle$. Assuming no band crossings, and given that $\langle N\mathbf{q}|\boldsymbol{\nabla} H_{N\mathbf{q}}|N\mathbf{q}\rangle = \boldsymbol{\nabla} E_{N\mathbf{q}}$, the right-hand side of the previous expression does not have any projection onto $|N\mathbf{q}\rangle$. Thus one can safely act on it with $(H_{N\mathbf{q}} - E_{N\mathbf{q}})^{-1}$, and determine $|\boldsymbol{\nabla} N\mathbf{q}\rangle$. This leads to $\boldsymbol{\Omega}_{N\mathbf{q}} = -\mathrm{Im}\langle N\mathbf{q}|(\boldsymbol{\nabla} E_{N\mathbf{q}} - \boldsymbol{\nabla} H_{N\mathbf{q}})(H_{N\mathbf{q}} - E_{N\mathbf{q}})^{-1}\times (H_{N\mathbf{q}} - E_{N\mathbf{q}})^{-1}(\boldsymbol{\nabla} E_{N\mathbf{q}} - \boldsymbol{\nabla} H_{N\mathbf{q}})|N\mathbf{q}\rangle$. Then, by plugging the identity operator $\mathcal{I}$ across the cross product, and noting that the left and right sides of the cross product do not have any projections onto $\langle N\mathbf{q}|$ and $|N\mathbf{q}\rangle$, respectively, one finds

$$\boldsymbol{\Omega}_{N\mathbf{q}} = -\mathrm{Im}\sum_{M\neq N}\frac{\langle N\mathbf{q}|\boldsymbol{\nabla} H_{N\mathbf{q}}|M\mathbf{q}\rangle\times\langle M\mathbf{q}|\boldsymbol{\nabla} H_{N\mathbf{q}}|N\mathbf{q}\rangle}{(E_{M\mathbf{q}} - E_{N\mathbf{q}})^2}, \tag{22}$$

through some simple algebra. In particular, for a two-dimensional system lying in the xy plane, e.g., in the Haldane-Hubbard model, $\boldsymbol{\Omega}_{N\mathbf{q}} = \Omega_{N\mathbf{q}}\widehat{\boldsymbol{k}}$ is along the z direction.

Appendix C: Isolated flat bands

Here we consider a number of weakly-coupled degenerate dispersionless flat bands that are energetically isolated from the rest of the Bloch bands in the spectrum [22]. Suppose $\varepsilon_{n\sigma\mathbf{k}} = 0$ is the energy of these flat bands, and they are separated by an energy ε_0 from the nearest band. In this case Eq. (5) reduces to $H^{\alpha\beta}_{N\mathbf{q}} \to H^{\alpha\beta}_{\mathbf{q}}$ where

$$H^{\alpha\beta}_{\mathbf{q}} = -\frac{U}{M_c}\sum_{nm\mathbf{k}} n^*_{\beta\uparrow\mathbf{k}+\mathbf{q}} m^*_{\beta\downarrow-\mathbf{k}} m_{\alpha\downarrow-\mathbf{k}} n_{\alpha\uparrow\mathbf{k}+\mathbf{q}}. \tag{23}$$

This effective Hamiltonian is valid only in the $U/\varepsilon_0 \to 0$ limit so that the dispersive bands can be projected out of the system. In the presence of time-reversal symmetry, i.e., when $n^*_{\alpha\downarrow-\mathbf{k}} = n_{\alpha\uparrow\mathbf{k}} \equiv n_{\alpha\mathbf{k}}$ and $\varepsilon_{n\downarrow-\mathbf{k}} = \varepsilon_{n\uparrow\mathbf{k}} \equiv \varepsilon_{n\mathbf{k}}$, we note that $H^{\alpha\beta}_{\mathbf{q}}$ is precisely the exact many-body Hamiltonian Eq. (13) that is derived in Ref. [22] under the same settings. This coincidence suggests that the interaction between the resultant two-body bound states, i.e., Cooper pairs, is negligible. Furthermore, since $H^{\alpha\beta}_{\mathbf{q}}$ does not depend on $E_{N\mathbf{q}}$ in this particular setting, the orthonormality condition is automatically intact for the resultant eigenvectors.

[1] A. Bansil, H. Lin, and T. Das, Colloquium: Topological band theory, Rev. Mod. Phys. **88**, 021004 (2016).
[2] F. D. M. Haldane, Model for a quantum Hall effect without Landau levels: Condensed-matter realization of the 'parity anomaly', Phys. Rev. Lett. **61**, 2015 (1988).
[3] G. Jotzu, M. Messer, R. Desbuquois, M. Lebrat, T. Uehlinger, D. Greif, and T. Esslinger, Experimental realization of the topological Haldane model with ultracold fermions, Nature **515**, 237 (2014).
[4] N. R. Cooper, J. Dalibard, and I. B. Spielman, Topological bands for ultracold atoms, Rev. Mod. Phys. **91**, 015005 (2019).
[5] Z. Liu and E. J. Bergholtz, Recent developments in fractional chern insulators (2022), arXiv:2208.08449.
[6] S. Rachel, Interacting topological insulators: a review, Reports on Progress in Physics **81**, 116501 (2018).
[7] N. Okuma and T. Mizoguchi, Relationship between two-particle topology and fractional Chern insulator, Phys. Rev. Res. **5**, 013112 (2023).
[8] H. Guo and S.-Q. Shen, Topological phase in a one-dimensional interacting fermion system, Phys. Rev. B **84**, 195107 (2011).
[9] M. A. Gorlach and A. N. Poddubny, Topological edge states of bound photon pairs, Phys. Rev. A **95**, 053866 (2017).
[10] A. Marques and R. Dias, Topological bound states in interacting Su–Schrieffer–Heeger rings, Journal of Physics: Condensed Matter **30**, 305601 (2018).
[11] G. Salerno, M. Di Liberto, C. Menotti, and I. Carusotto, Topological two-body bound states in the interacting Haldane model, Phys. Rev. A **97**, 013637 (2018).
[12] L. Lin, Y. Ke, and C. Lee, Interaction-induced topological bound states and Thouless pumping in a one-dimensional optical lattice, Phys. Rev. A **101**, 023620 (2020).

[13] J. Zurita, C. E. Creffield, and G. Platero, Topology and interactions in the photonic Creutz and Creutz-Hubbard ladders, Advanced Quantum Technologies **3**, 1900105 (2020).

[14] G. Salerno, G. Palumbo, N. Goldman, and M. Di Liberto, Interaction-induced lattices for bound states: Designing flat bands, quantized pumps, and higher-order topological insulators for doublons, Phys. Rev. Res. **2**, 013348 (2020).

[15] G. Pelegrí, A. M. Marques, V. Ahufinger, J. Mompart, and R. G. Dias, Interaction-induced topological properties of two bosons in flat-band systems, Phys. Rev. Res. **2**, 033267 (2020).

[16] M. Iskin, Two-body problem in a multiband lattice and the role of quantum geometry, Phys. Rev. A **103**, 053311 (2021).

[17] M. Iskin and A. Keleş, Stability of $(N+1)$-body fermion clusters in a multiband Hubbard model, Phys. Rev. A **106**, 033304 (2022).

[18] M. Iskin and A. Keleş, Dimers, trimers, tetramers, and other multimers in a multiband Bose-Hubbard model, Phys. Rev. A **106**, 043315 (2022).

[19] J.-X. Yin, B. Lian, and M. Z. Hasan, Topological kagome magnets and superconductors, Nature **612**, 647 (2022).

[20] M. Kang, L. Ye, S. Fang, J.-S. You, A. Levitan, M. Han, J. I. Facio, C. Jozwiak, A. Bostwick, E. Rotenberg, *et al.*, Dirac fermions and flat bands in the ideal kagome metal FeSn, Nature materials **19**, 163 (2020).

[21] L. Balents, C. R. Dean, D. K. Efetov, and A. F. Young, Superconductivity and strong correlations in Moiré flat bands, Nature Physics **16**, 725 (2020).

[22] J. Herzog-Arbeitman, A. Chew, K.-E. Huhtinen, P. Törmä, and B. A. Bernevig, Many-body superconductivity in topological flat bands (2022), arXiv:2209.00007.

[23] As far as the two-body problem is concerned, there is no essential difference between the results of Bose-Hubbard and Fermi-Hubbard models when $h_{\sigma\mathbf{k}} \equiv h_{\mathbf{k}}$ in the latter [17, 18].

[24] W. P. Su, J. R. Schrieffer, and A. J. Heeger, Solitons in polyacetylene, Phys. Rev. Lett. **42**, 1698 (1979).

[25] M. Di Liberto, A. Recati, I. Carusotto, and C. Menotti, Two-body physics in the Su-Schrieffer-Heeger model, Phys. Rev. A **94**, 062704 (2016).

[26] L. Lin, Y. Ke, and C. Lee, Interaction-induced topological bound states and Thouless pumping in a one-dimensional optical lattice, Phys. Rev. A **101**, 023620 (2020).

[27] D. R. Hofstadter, Energy levels and wave functions of bloch electrons in rational and irrational magnetic fields, Phys. Rev. B **14**, 2239 (1976).

[28] D. Cocks, P. P. Orth, S. Rachel, M. Buchhold, K. Le Hur, and W. Hofstetter, Time-reversal-invariant Hofstadter-Hubbard model with ultracold fermions, Phys. Rev. Lett. **109**, 205303 (2012).

[29] D. Shaffer, J. Wang, and L. H. Santos, Theory of Hofstadter superconductors, Phys. Rev. B **104**, 184501 (2021).

[30] R. Umucalılar and M. Iskin, BCS theory of time-reversal-symmetric Hofstadter-Hubbard model, Physical Review Letters **119**, 085301 (2017).

[31] We are not aware of any study on the topological phase diagram of the generalized Haldane model, where next-nearest-neighbor (i.e., intra-sublattice) hoppings are different for different sublattices, to compare our two-body results.

[32] T. Fukui, Y. Hatsugai, and H. Suzuki, Chern numbers in discretized Brillouin zone: efficient method of computing (spin) Hall conductances, Journal of the Physical Society of Japan **74**, 1674 (2005).

[33] M. V. Berry, Quantal phase factors accompanying adiabatic changes, Proceedings of the Royal Society of London. A. Mathematical and Physical Sciences **392**, 45 (1984).